A Robust Meshing and Calibration Approach for Sensorless Freehand 3D Ultrasound

Hassan Rivaz[a], Emad Boctor[a], and Gabor Fichtinger[a,b,c]

Department of [a]Computer Science, [b]Mechanical Engineering, [c]Radiology,
Johns Hopkins University

ABSTRACT

The elevational distance between two ultrasound images can be obtained from the correlation between the two images, leading to sensorless freehand 3D ultrasound systems. Most of these systems rely on the correlation between patches of fully developed speckles (FDS). Previous work[1] has compared different FDS detectors and concluded that the elevational distance measurement limited to the FDS patches obtained by low order moment test yields significantly more accurate results than other FDS detectors. However, small coherent and FDS regions are spread throughout a typical ultrasound image of real tissue. This makes it extremely unlikely to find a regularly shaped (conventionally a rectangle) FDS patch, making it infeasible to estimate elevational distance accurately.[1] In this work, first we propose a simple and fast algorithm which is capable of detecting arbitrarily irregular FDS regions in an ultrasound image. In vitro experiments on beef liver, beef steak and chicken breast indicates that the proposed algorithm generates remarkably more FDS patches than the current methods. Preliminary results show that the FDS patches obtained by this algorithm generate more accurate elevational distance measurement. Second, we propose a new calibration scheme to generate decorrelation curves. At a particular location in the image, conventional methods acquire one decorrelation curve. We create multiple curves, as a function of particular statistical properties of the patch. The results reveal a theoretically expected relation between the decorrelation curve and the statistical properties of the patch. As a result of this calibration based on the patch statistical properties, improvement in the out of plane motion estimation is expected.

Keywords: 3D ultrasound, Speckle decorrelation, Fully developed speckle

1. INTRODUCTION

Current technology allows acquiring 3D ultrasound data either using oscillating head probes or freehand 3D ultrasound. In oscillating head probes, a 1D ultrasound transducer is automatically swept inside the probe, enabling 3D image acquisition. In freehand 3D ultrasound, a position sensor is attached to an ordinary probe which is swept over the desire region by the clinician.

Freehand 3D ultrasound is inexpensive, works with the existing 2D probes, and allows arbitrary 3D volume acquisition. However, the need for the additional sensor makes it difficult to use. Sensorless volume reconstruction of freehand 3D ultrasound is possible using the information in the images themselves: out of plane motion estimation can be obtained from image correlation,[2] which is the focus of this work, while in plane motion can be estimated through image registration.[3–5]

Granular apperance of ultrasound images is the key factor in out-of-plane motion estimation. Each pixel in an ultrasound image is formed by the back scattered echoes from an approximately ellipsoid called the resolution cell (Figure 1). The interference of scatterers in a resolution cell creates the granular appearance of the ultrasound image, called speckle. Although of random appearance, speckle pattern is identical if the same object is scanned from the same direction and under the same focusing and frequency.

Further author information: (Send correspondence to E-mail: {rivaz, eboctor, gabor}@cs.jhu.edu

Medical Imaging 2007: Ultrasonic Imaging and Signal Processing, edited by
Stanislav Y. Emelianov, Stephen A. McAleavey, Proc. of SPIE Vol. 6513,
651318, (2007) · 1605-7422/07/$18 · doi: 10.1117/12.712423

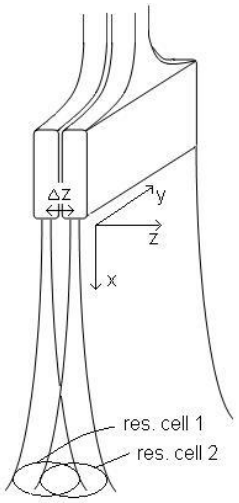

Figure 1. Aquisition of two ultrasound images at a distance of Δz. Ultrasound beam is in order of a millimeter wide. This wideness affects the resolution of ultrasound image in the lateral, y, and elevational, z, directions, as well as creating a granular pattern, called speckle. The size of the resolution cell in the axial direction, x, is determined by the wavelength of the ultrasound wave and is magnified in this image.

Each pixel in the ultrasound image is created by the backscattered echoes from the resolution cell. If two images are acquired at a small enough elevational distance,[6,7] their corresponding resolution cells share some overlapped volume (Figure 1) and therefore some scatterers. Thus, the pixels brightness of such two images are correlated. The correlation can be used along with a decorrelation curve, obtained by a acquiring images of a FDS phantom at small elevational steps , to calculate the elevational distance.[2] Since the wideness of ultrasound beam varies axially and laterally, multiple decorrelation curves are usually obtained for patches of image located at different axial and lateral positions.

Coherent scattering causes the elevational distance measurement from the conventional correlation algorithms to be underestimated.[1] Thus, distance measurement is limited to the patches of the ultrasound image that contain only FDS.[1] To completely determine the out-of-plane degrees of freedom between two planes, at least three non-collinear pairs of such patches are required.[5]

Since FDS patches are extremely rare in real tissue, these methods usually have a low accuracy and are only relevant in limited tissue types. Gee et al.[8] proposed a heuristic technique that is robust to the lack of FDS patches in the ultrasound image. This method allows the calculation of the elevational distance for all patches of the image, regardless of their level of coherency, by measuring the axial and lateral correlation of each patch. Since the behavior of coherent reflectors in the elevational direction can be different from their behavior in the axial and lateral directions, the performance of the method can decline depending on the level of anisotropy of the tissue. The purpose of this work is to devise a method applicable to a various tissue types that accurately reconstructs 3D volumes from ultrasound images.

We perform a two-step meshing scheme to reduce the level of the coherency of the image patches. We use signal to noise ratio and skewness of data, same as the statistics that are used in the calibration, in both steps.[9] This step allows us to segment irregularly shaped patches that have low coherency.

Having a set of decorrelation curves as a function of coherent scattering would also potentially improve the elevational distance measurement. However, acquiring such a set would require thousands of calibration experiments performed on phantoms with different coherent scattering properties. We cope this problem by performing the calibration on a "low quality" phantom as described in the next section.

2. CREATING IMAGE PATCHES WITH LOW COHERENCY

To calculate the elevational distance between two ultrasound frames, image patches with low coherency from the two frames are required. We use low order moments to classify speckle:

$$R = \text{SNR} = \frac{\langle A^{v_r} \rangle}{\sqrt{\langle A^{2v_r} \rangle - \langle A^{v_r} \rangle^2}} \tag{1}$$

$$S = \text{skewness} = \frac{\left\langle (A^{v_s} - \langle A^{v_s} \rangle)^3 \right\rangle}{(\langle A^{2v_s} \rangle - \langle A^{v_s} \rangle^2)^{\frac{3}{2}}} \tag{2}$$

where A is the amplitude of the ultrasound RF envelope, v_r and v_s are the signal powers and $\langle \cdots \rangle$ denotes the mean. Here we use[9] $v_r = 2v_s = 1$. R and S of a image patch which contains few thousand pixels, depending on the correlation of pixels in the patch,[10] are calculated. If the R and S duple falls inside an elliptical FDS discriminative function, the patch is considered to contain FDS. The ratio of the distance of the R and S duple from the center of the FDS ellipse to the radius of the ellipse in the point's direction, ϑ, may be used to quantify the closeness of a patch to FDS.

To best of our knowledge, current freehand 3D systems work with rectangular patches. However, small coherent and FDS regions are spread throughout a typical ultrasound image of real tissue. This makes it extremely unlikely to find a regularly shaped, i.e. rectangular, FDS patch. We propose a simple and fast two-step meshing algorithm which is capable of detecting arbitrarily irregular FDS regions in an ultrasound image.

2.1. Two-Step Meshing Algorithm

To classify a patch reliably, it should contain thousands of data samples. However, some small patches are very coherent and they can be classified as non-FDS with much fewer data samples. This is the inspiration for the two-step meshing algorithm. We elaborate the algorithm with using an ultrasound image of beef liver (Figure 2). The size of this image is (r x c) = (1500 x 500), where r stands for row and c for column. Approximately 3600 samples are required to classify a patch in this image.

In the first step, the image is divided into small patches of ($r1$ x $c1$)=(50 x 10) containing 500 samples (Figure 2 a). Because of the small sample size, patches cannot be classified reliably and false acceptances and rejections are likely in this stage. However, it is possible to eliminate patches that are very far from FDS (large ϑ). We mark patches with $\vartheta < 5$ as potential FDS. The mesh is then shifted by (rs x cs)=(10 x 2) pixels, where rs and cs stand for row shift and column shift, and the speckle classification is performed. The shifting process is repeated for $\frac{r1}{rs} \times \frac{c1}{cs} = 25$ times. This will create a very fine grid of size rs x cs where each patch can be classified as a FDS potential for $\frac{r1}{rs} \times \frac{c1}{cs}$ times. We then mark the fine patches that are identified as FDS potential less than a threshold $TH = 4$ as non-FDS (black regions in Figure 2 b).

In the second step, we overlay the final mesh of size ($r2$ x $c2$)=(75 x 125) on the output of step 1. We then search for patches with $\vartheta < 4$ that contain more than 7500 non-black pixels (Figure 2 c). Three such patches are found in the image , while a conventional method finds one patch with $\vartheta < 4$.

Figure 3 shows the performance of the two-step meshing algorithm in the R-S plane. Comparing to the results of a one-step mesh, the two-step mesh generates remarkably more patches close to the FDS ellipse. We have found similar results with chicken breast and beef steak.

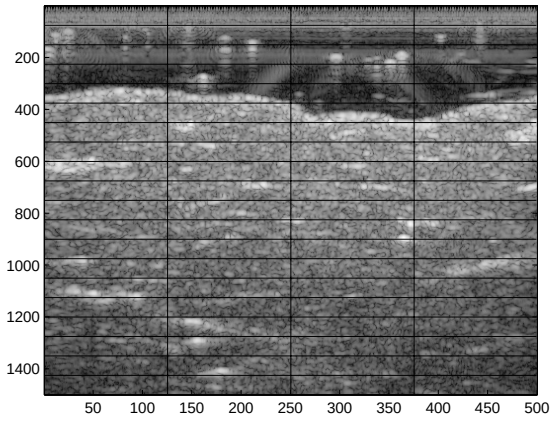

(a) Original B-mode.

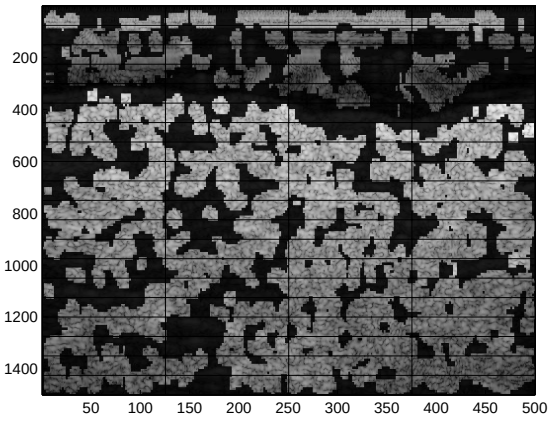

(b) Potential FDS parts.

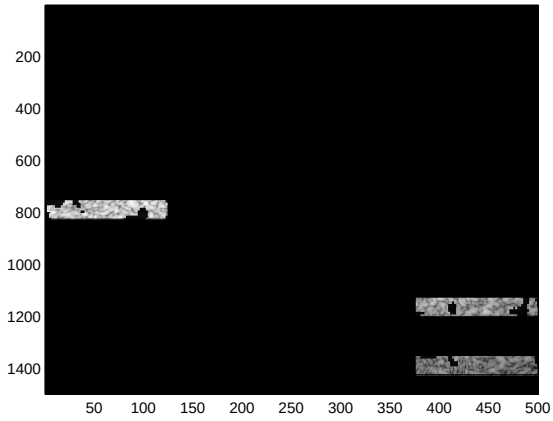

(c) FDS patches.

Figure 2. The two-step meshing algorithm. (a) shows the original B-mode image of beef liver. (b) shows the output of the first step of the algorithm. (c) shows the three FDS patches found in the image. The ($r2$ x $c2$)=(75 x 125) grid is superimposed in the parts (a) and (b) only to ease comparison with part (c).

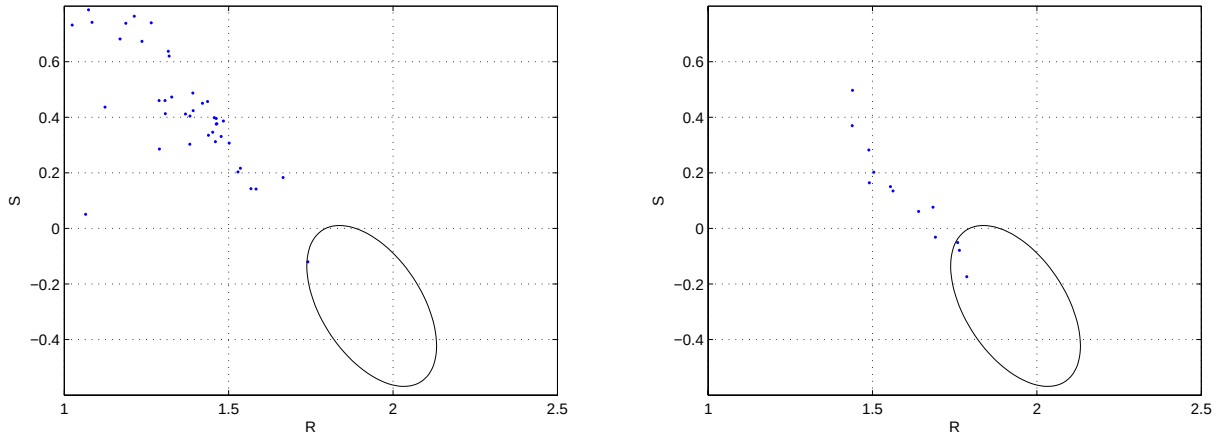

(a) One-step meshing.

(b) Two-step meshing.

Figure 3. The comparison of one-step mesh and two-step mesh using beef liver image of Figure 2 (a). (a) shows the R-S values of a 75 x 100 grid and (b) shows the R-S values of the two-step meshing algorithm with parameter values as described before. In (a) only points close to the ellipse and in (b) only R-S of the patches that contain more than 7500 pixels are shown. The radius of the ellipse is magnified by $\vartheta = 4$.

3. ELEVATIONAL MOTION ESTIMATION

In this section, we first acquire the decorrelation curves, i.e. estimate the size of the resolution cell, at different locations of the image using a FDS phantom. We then use the decorrelation curves, along with the irregular patches that are found using the method described in the previous section, to estimate the elevational distance motion of an in-vitro beef liver experiment.

3.1. Acquiring decorrelation curves in a FDS phantom

A Siemens Antares ultrasound machine with research interface is used to acquire RF data. Homogeneous parts of a CIRS elasticity QA phantom (CIRS, Norfolk, VA, USA) is used as the FDS phantom. 60 image frames are acquired at $\delta z = 0.05$mm elevational distance, each image 20mm deep with a single focus at 5mm depth at 6.67MHz frequency. Each image consists of 508 RF lines, with each RF line containing 1500 samples. The images are filtered using a 4.67-8.67 MHz passband Butterworth filter.

The correlations are calculated using Pearsons linear correlation coefficient ρ

$$\rho(X,Y) = \frac{N\Sigma x_i y_i - \mu_x \mu_y}{\sqrt{\left(N\Sigma x_i^2 - \mu_x^2\right)\left(N\Sigma y_i^2 - \mu_y^2\right)}} \tag{3}$$

where x_i and y_i, $i = 1 \cdots N$, are the magnitude of the RF data from patches X and Y and μ_x and μ_y are the means of patches X and Y respectively. Because of the high level of correlation in the image data in the lateral and axial directions, each patch consists of 75 pixels in the axial direction and 100 pixels in the lateral direction, containing 7500 data samples. 20 x 5 decorrelation curves are calculated and are used in the next step to estimate out of plane motion of the probe.

3.2. Using the irregular FDS patches to estimate motion

17 image frames are acquired from beef liver at $\Delta z = 0.05$mm elevational distance. The imaging parameters and parameters of the two-step meshing algorithm are as mentioned before. The correlation between corresponding FDS patches in frames i and j is used to calculate their elevational distance. We "stitch" the two frames i and j and search for FDS patches which now consist of pixels from both frames. This will guarantee finding

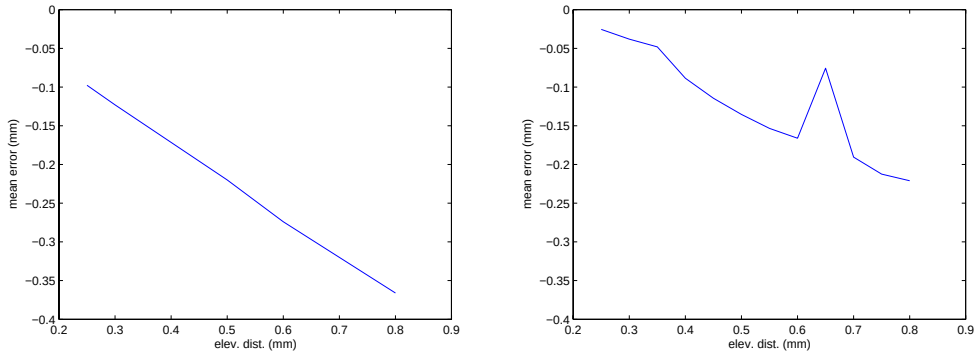

(a) One-step mesh.

(b) Two-step mesh.

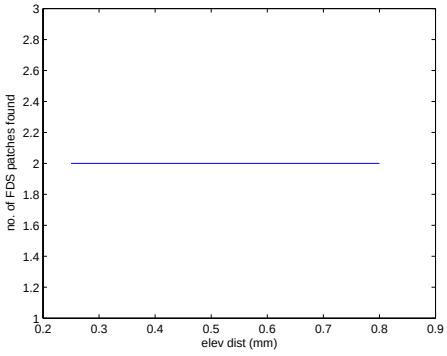

(c) One-step mesh.

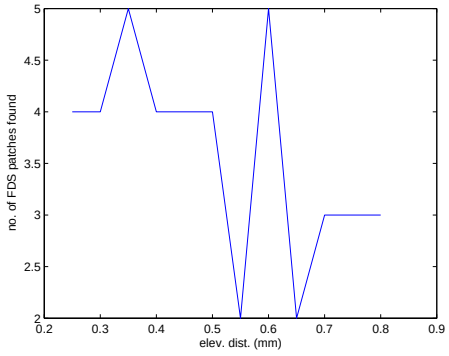

(d) Two-step mesh.

Figure 4. (a) shows the difference of the distance calculated from the mean of the two distances obtained from the two FDS patches found from the actual distance and (b) shows the same value using two-step mesh. (c) and (d) show the number of FDS patches found in each case.

corresponding FDS patches in the two frames.

Unlike a one-step mesh, the output of the two-step mesh is patches that are not at the same place where decorrelation curves are calculated. As a result, we calculate the center of gravity (CG) of each FDS patch and linearly interpolate the two calibration curves on top and bottom of the CG to obtain the calibration curve for the FDS patch.

Figure 4 (a) and (b) show the error of the estimated distance using regular meshing and the two-step meshing algorithm. The threshold ϑ in the regular meshing algorithm is set such that at least one FDS patch is found between each two frames. The x-axis is the exact value of the distance between two frames and the y-axis shows the error in the measurement. The two step meshing algorithm has increased the accuracy by a factor of almost two. Figure 4 (c) and (d) shows the number of FDS patches found in each case. In addition to the more accuracy, more patches are found in the two-step meshing algorithm which is important in determining the 3D orientation of two image frames.

By inspecting all the distances measured from the FDS patches, we realize that 2 patches give very accurate distance estimation (patches found from frames 1 and 13 at x=0.65mm in Figure 4 (b) and (d)), while three other patches give a non-accurate estimation. We expect to increase the accuracy of the two step meshing algorithm by adding other statistical parameters to the R-S to classify speckles, since the R-S test fails to reject some coherent patches. Particularly, the axial and lateral correlation of a patch at a known axial and lateral displacement are expected to decrease false positive FDS detection and therefore increase the level of accuracy.

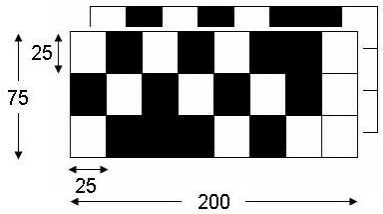

Figure 5. An example of the selection of 12 patches from the 24 small patches such that each of the 3 rows contains 4 patches.

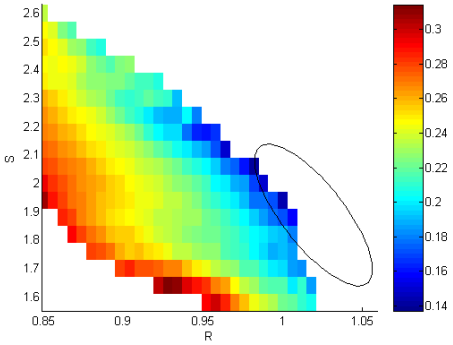

Figure 6. Correlation as a function of R and S. Different pixels of two frames of beef liver, acquired at $\Delta z = 0.8$mm, are selected as depicted in Figure 4 to obtain a statistics dependent calibration.

4. THE CALIBRATION APPROACH

Current sensorless freehand 3D ultrasound systems perform the calibration only for FDS patches. This is because it is practically impossible to make hundreds of different phantoms with different properties and obtain calibration curve as a function of statistical properties. We obtain the decorrelation curves as a function of R-S, i.e. the level of coherency as follows.

Consider two patches of frames i and j, at a known Δz distance, each containing 75 x 200 pixels (Figure 4). Half of the pixels of each patch is required to calculate the correlation between the two patches assuming that we need 7500 data samples in each patch. Divide each patch to smaller patches of size 25 x 25, resulting in 3 x 8 patches as depicted in the figure. Now we choose 4 patches from the 8 patches in each row, 12 patches out of the 24 in total. This selection is possible in $\binom{8}{4}^3 = 343000$ different ways, and therefore 343000 different R-S values. For each selected patch, we calculate the correlation between the two patches and average the values in the R-S plane.

Figure 6 is a result of such an averaging on two patches from two image frames of beef liver $\Delta z = 0.8$mm apart. The calibration result show an increase in the correlation as the R-S value of the patch moves further from the FDS ellipse. This is in accordance with physics of ultrasound, resulting in an expected increase of the accuracy of motion estimation.

5. DISCUSSION AND CONCLUSIONS

In-vitro experiments on real tissue shows that the two-step meshing algorithm is substantially effective in eliminating coherent parts of the image and finding low coherency patches. Preliminary experiments show that such low coherency patches result in a 50% increase in the accuracy of out of plane motion estimation using image correlation compared to a conventional one-step mesh. Adding other statistical measures, such as correlations in the lateral and axial directions will decrease the false positive probability of the R-S speckle classifier.

The linear interpolation step to obtain the decorrelation curve at the center of gravity of the FDS patches increases the uncertainty of the decorrelation curves. Future research will consider other approaches to acquire the calibration curve for the FDS patches found in the experiment.

The calibration approach based on the statistics of the patch is expected to increase the accuracy of motion estimation. It will also help to eliminate the need for a FDS phantom for calibration. Given the novel meshing and calibration approaches, accurate and robust motion estimation in real tissue will be possible, eliminating the need for an external sensor in freehand 3D ultrasound systems.

ACKNOWLEDGMENTS

This research is supported by core NSF CISST/ERC EEC-9731478. The authors also acknowledge Siemens Corporate Research.

REFERENCES

1. P. Hassenpflug, R. Prager, G. Treece, and A. Gee, "Speckle classification for sensorless freehand 3-d ultrasound," *Ultrasound in Med. and Biol.* **31**, pp. 1499–1508, November 2005.
2. J. Chen, B. Fowlkes, P. Carson, and J. Rubin, "Determination of scan-plane motion using speckle decorrelation: theoretical considerations and initial test," *Imag. Sys. and Tech.* **8**, pp. 38–44, 1997.
3. G. Treece, R. Prager, A. Gee, C. Cash, and L. Berman, "Correction of probe pressure artifacts in freehand 3d ultrasound," *Medical Image Analysis* **6**, pp. 199–215, 2002.
4. B. Geiman, L. Bohs, M. Anderson, S. Breit, and T. G.E., "A novel interpolation strategy for estimating subsample speckle motion," *Pattern Recog. Letters* **45**, pp. 1541–1552, 2002.
5. R. Prager, A. Gee, G. Treece, C. Cash, and L. Berman, "Sensorless freehand 3-d ultrasound using regression of the echo intensity," *Ultrasound in Med. and Biol.* **29**, pp. 437–446, 2003.
6. W. Smith and A. Fenster, "Optimum scan spacing for three-dimensional ultrasound by speckle statistics," *Ultrasound in Med. and Biol.* **26**, pp. 551–562, May 2000.
7. W. Smith and A. Fenster, "Analysis of an image-based transducer tracking system for 3d ultrasound," *Proceedings of SPIE - The International Society for Optical Engineering* **5035**, pp. 154–165, 2003.
8. A. Gee, R. Houdson, P. Hassenpflug, G. Treece, and R. Prager, "Sensorless freehand 3d ultrasound in real tissue: Speckle decorrelation without fully developed speckle," *Medical Image Analysis* **10**, p. 137:149, April 2006.
9. H. Rivaz, E. Boctor, and G. Fichtinger, "Ultrasound speckle detection using low order moments," in *IEEE Int. Ultrasonics Symp.*, p. in press, 2006.
10. V. Dutt and J. Greanleaf, "Speckle analysis using signal to noise ratios based on fractional order moments," *Ultrasonic Imag.* **17**, pp. 251–268, 1995.